CFD Applied to the Simulation of the Vibration Phenomenon Due to the Cadenced Shedding of Vortices in a Circular Cylinder

Alexandre Miguel Silva Araújo[1], Juliema Fronczak[1], Karin Kauss[1], Marcelo Caetano Monteiro[1], Bruno Giudice Batista de Araujo Porto[1], Gabriel Antonio Mendes das Flores[1], Mariana Reis Pereira[2], Patricia Habib Hallak[3]

[1]*Postgraduate Program in Civil Engineering, Federal University of Juiz de Fora*
José Lourenço Kelmer Street, São Pedro, 36036-900, Minas Gerais/Juiz de Fora, Brazil
araujo.alexandre@engenharia.ufjf.br, juliema.fronczak@engenharia.ufjf.br, karin.kauss@engenharia.ufjf.br
marcelo.monteiro@engenharia.ufjf.br, bruno.porto@engenharia.ufjf.br, gabriel.flores@engenharia.ufjf.br
[2]*Graduate in Civil Engineering, Federal University of Juiz de Fora*
José Lourenço Kelmer Street, São Pedro, 36036-900, Minas Gerais/Juiz de Fora, Brazil
mariana.reis@engenharia.ufjf.br
[3]*Dept. of Computational and Applied Mechanics, Federal University of Juiz de Fora*
José Lourenço Kelmer Street, São Pedro, 36036-900, Minas Gerais/Juiz de Fora, Brazil
patricia.hallak@ufjf.edu.br

Abstract. The formation of vortex is related to the separation of the boundary layer close to the immersed body, depending on the pressure distribution. The aeroelastic phenomenon, known as vortex-induced vibration (VIV), occurs when the shedding frequency of these vortex approaches one of the structures natural frequencies. Its study is of practical interest in many branches of engineering, such as risers, bridges, and aeronautical profiles. In this work, the VIV around a circular cylinder was analyzed numerically through CFD (Computational Fluid Dynamics) simulations. The numerical method is described by solving the incompressible Navier-Stokes equations in a Lagrangian-Eulerian framework in a two-dimensional geometric model. In this study, the open-source OpenFOAM® was used. The numerical experiments were carried out in a cylinder with a unit diameter, with Reynolds number values of 100, 200, and 400, for reduced velocitys *Ur* from 1 to 13, and a damping rate ranging from 0 %$\leq \xi \leq$5%. The movement of the cylinder is described using a mass-spring-damper system. For the cylinder movement, the sixDoFRigidDisplacement solver was used and the solution algorithm for pressure-velocity coupling was the pimpleFoam. The results of the simulations were consistent when compared to the literature. It is observed that the damping factor affects the responses of the cylinder, depending on the reduced velocity. It is also observed that the movement of the cylinder significantly affects the flow field, varying parameters such as Strouhal, drag coefficient, lift coefficient, and pressure on the studied surfaces. Finally, it was concluded that the results were satisfactory and that the proposed computational model is a useful tool in solving problems involving the phenomenon of vortex-induced vibration.

Keywords: CFD, circular cylinder, VIV, OpenFOAM, simulation.

1 Introduction

Understanding the flow around a circular cylinder has been a fundamental challenge for researchers, in large part due to the complexity and transient nature of the fluid. However, in the last decade, computational resources have evolved enough that high-resolution solutions for practical engineering have become viable, such as simulation in Computational Fluid Dynamics (Stringer et al., 2014) [1].

The simulation done in CFD software allows to observe the phenomena in a more realistic way, and also allows the reduction of expenses in relation to experiments because, through CFD, it is possible to evaluate several tests in simulations for a certain improvement in the process and select only those that get better results to run (Cóstola and Alucci, 2014) [2].

The study of fluid flow around circular cylinders has been studied over the years. Many experimental and

numerical works published in the literature on the flow past in cylinders were carried out, due to the great interest in studying and predicting the flow behavior around the cylinder, due to its wide application in engineering (Palau-Salvador et al., 2010) [3].

Vortex-induced vibration of a circular cylinder in constant flow has been intensively investigated in the last two decades. Comprehensive reviews of VIV, which seek to understand the relationship between cylinder movement and vortex shedding flow, can be found in many publications, such as Sarpkaya (1979) [4], Bearman (1984) [5], Brika and Laneville (1993) [6], Sarpkaya (2004) [7], Belloli et al. (2015) [8].

Considering the complexity found in a preliminary research of the object of study, the simplification of the problem regarding its degrees of freedom is justified. Thus, the circular cylinder at one degree of freedom was studied.

Initially, the study was carried out with the fixed cylinder, in order to perform a mesh test and, later, simulations of VIV were carried out with the spring-mass and spring-mass-damper systems, using the Unsteady Reynolds Average Navier-Stokes method (URANS) and, finally, the effectiveness of the executed approach was verified, validating the obtained results comparing them with the available literature.

2 Theoretical basis

2.1 Governing equations in fluid dynamics

An incompressible and viscous flow, with the characteristics of those simulated here, can be described by the physical and mathematical model of the Navier Stokes equations representing the balance of momentum and by the equation of the principle of conservation of mass, familiarly known as the equation of continuity:

$$\nabla.\vec{v} = 0, \tag{1}$$

$$\rho\frac{\partial\vec{v}}{\partial t} + \rho\nabla.\vec{v}\vec{v} = -\nabla.p + \nabla.(\bar{\bar{\tau}}) + \rho\vec{g} + \vec{F}. \tag{2}$$

In the equations above, ρ is the density of the fluid; p, the pressure; μ, is viscosity; $\vec{v}$ the velocity field; $\widetilde{\bar{\tau}} = \mu\left[\left(\nabla\vec{v} + \nabla\vec{v}^T\right)\right]$ is the stress tensor; $\rho\vec{g}$ and $\vec{F}$ are gravitational and external forces, respectively.

2.2 Vortex-Induced Vibrations Phenomenon

Strouhal proposed in 1878 that the regularity of vortex shedding phenomena can be described in terms of a dimensionless number:

$$St = \frac{f_s D}{U_0} \tag{3}$$

Where *St* is the Strouhal number; and the f_s, *D* and V_0 are, respectively, the frequency of vortex shedding, the dimension of the body through which the flow passes, and the uniform mean velocity of the flow. Vortex-induced vibrations result from a very complex phenomenon, as they are inherent to the dynamic characteristics of the structure such as mass, rigidity, damping, and geometry, but it also depends on the characteristics of the flow itself, kinematic viscosity and velocity. It is through this fluid-structure interaction that the system vibrates.

In accordance with Blevins (2001) [9], the phenomenon of fluid-structure interaction is characterized as follows: the flow in contact with the structure exerts a displacement or deformation force, changing its orientation about the flow. When this change of orientation happens, it can alter the forces exerted by the flow and thus triggering a self-sustaining process of vibrations. An important characteristic of the phenomenon is the capture and synchronization of vortex shedding at the structure's natural flexural oscillation frequency, which occurs in the speed range for which the vibration amplitudes are greater.

3 Numerical techniques

The simulations were obtained using the OpenFOAM® program (Open Source Field Operation And Manipulation) which works in C++ language for the development of methods for solving continuum mechanics'problems, as well as CFD.

Discretization of the differential equations was performed by using the finite volume method. The PIMPLE scheme (Pressure Implicit with Splitting of Operators combined with SIMPLE) technique was used in a transient-state with an implicit scheme for advancing the time step, which allows explicit relaxations of variables and implicit

equations; this tool is used to advance the time step, a second-order scheme for solving convective and diffuse terms.

The movement of the cylinder is described according to a mass-spring-damper system. For the movement of the cylinder, the solver sixDoFRigidDisplacement was used, and for the solving of moving mesh problems, the displacementLaplacian solver was used.

4 Results

This section presents the computational domain and boundary conditions. In the sequence, two numerical examples are presented.

4.1 Computational domain and boundary conditions

In this study, the flow through the cylinder with a circular base was considered for a low Reynolds value. According to Vikram et al. (2014) [10], the choice of the domain through which the flow passes is still an art in CFD, whereas only a finite computational domain can be used in numerical simulation. Consequently, it is important to define the input and output domains far enough away from the main cylinder, so that the boundary conditions do not introduce any undesirable effects in the main region of interest, ie, around the cylinder.

The domains in this study are shown in Figures 1 and 2. Figure 1 represents the geometry of the cylinder with a circular base, which has a fixed unitary dimension. Figure 2 shows the mesh around the cylinder. For the entire outline, the second normal derivative of pressure is given as a reference mean of 0 Pa. All distances presented are dimensionless by the diameter of the cylinder in order to analyze the effect of the flow on the structure.

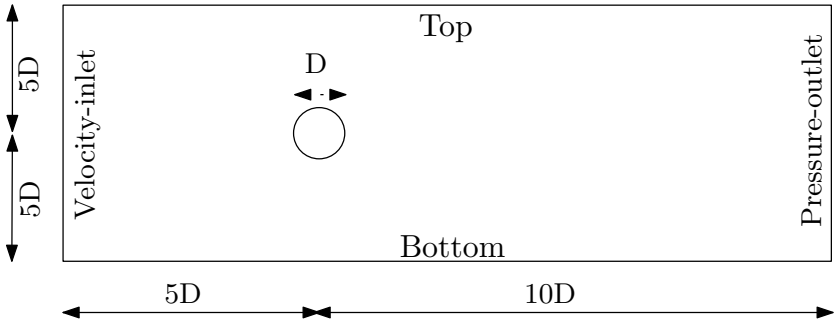

Figure 1. Fluid domain and boundary conditions

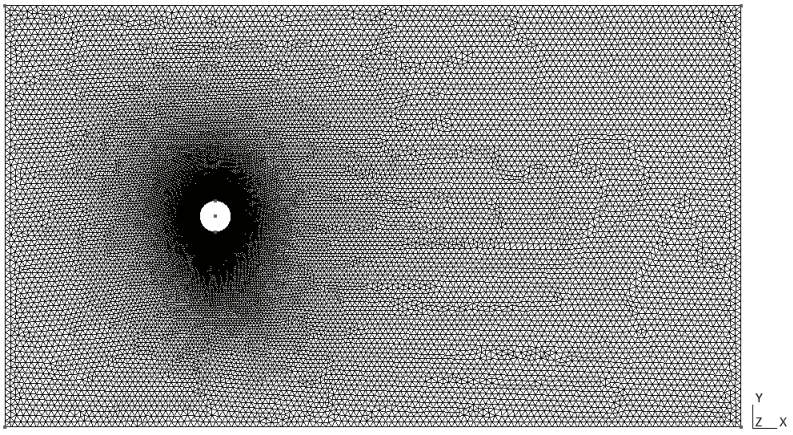

Figure 2. Unstructured mesh around cylinder

At the boundaries *Inlet, Top* and *Bottom*, uniform flow with unit velocity and zero pressure gradient were

assumed. In *Outlet*, the zero pressure and zero velocity gradient condition were applied. On the cylinder walls *Wall*, the non-slip condition, and the zero pressure gradient were applied.

4.2 Mesh independence test at static cases

In this section, the main results obtained with the mesh test performed are presented. In it, we sought to verify and validate the numerical simulations of constant uniform flow around a circular cylinder, with Reynolds ranging from 100, 200 and 400.

In order to reduce the computational cost, three meshes were proposed. Meshes have a computational domain of 15 elements horizontal and 10 elements vertical. Table 1 shows the characteristics of these meshes. The results of C_d, Cl_{rms} and St obtained from meshes 1, 2, and 3 of the fixed case simulations, together with the literature references, are presented in Table 2.

The dimensionless force coefficient, C_d, is used for quantify the resistance of an object to the passage of a fluid around a geometry, be it cylindrical, rectangular and others. It is a coefficient that does not show a constancy in its results, because when dimensionless it depends on the Reynolds number and other geometric dimensionless quantities.

Cl_{rms} is a dimensionless coefficient relating the lift generated by a geometry, the dynamic pressure of the fluid flow, and the associated reference area.

Table 1. Mesh independence test carried out for flow past a circular cylinder at static cases

Meshes	Mesh type	Elements (h $\times$ v)	Number of nodes / Elements	Aspect ratio	Skewness
Mesh 1	Unstructured	15×10	26786 / 11563	2.62	0.70
Mesh 2	Unstructured	15×10	60146 / 59391	2.40	0.48
Mesh 3	Structured	15×10	76680 / 102240	28.0	1.00

The results of the simulations can be seen in Table 2, below.

Table 2. Aerodynamic results

Meshes	Re = 100			Re = 200			Re = 400		
	$\overline{C_d}$	Cl_{rms}	St	$\overline{C_d}$	Cl_{rms}	St	$\overline{C_d}$	Cl_{rms}	St
Mesh 1	1.3788	0.2443	0.1709	1.4529	0.5092	0.2015	1.5232	0.8151	0.225
Mesh 2	1.3900	0.2423	0.1709	1.3807	0.5005	0.2014	1.4482	0.7853	0.2197
Mesh 3	1.4296	0.2161	0.1709	1.3813	0.4400	0.2075	1.4801	0.7844	0.2319
Literature review									
Stringer et al. (2014) [1]	1.4000	0.2400	0.1800	-	-	-	-	-	-
Junior L. B. (2007) [11]	1.3926	0.2416	0.1700	-	-	-	1.4403	0.7787	0.2233
Franke et al. (1990) [12]	-	-	-	1.3100	0.6500	0.1940	-	-	-

Analyzing the results, it is verified that the values C_d, Cl_{rms} e St vary with the refinement of the mesh, and that Mesh 1 (see Figure 2), intermediate, presented results closer to the literature. This, and also its lower computational cost, were the determining factors in its choice for the VIV simulation.

4.3 Mass-Spring-Damper System

Studies were carried out to investigate the importance of some parameters such as the ratio between the dominant oscillation frequency f and the natural frequency of the system f_s expressed in Figure 3; the maximum dimensionless amplitude Y of the system shown in Figure 4; the mean of the drag coefficient C_d and the fluctuation of the lift coefficient Cl_{rms} both expressed in Figure 5 and 6 respectively. All parameters were analyzed for a

spring-mass and spring-mass-damping system, with damping rates $\xi = 0$, $\xi = 0.01$ and $\xi = 0.05$, with one number of Reynolds 400 for all simulations.

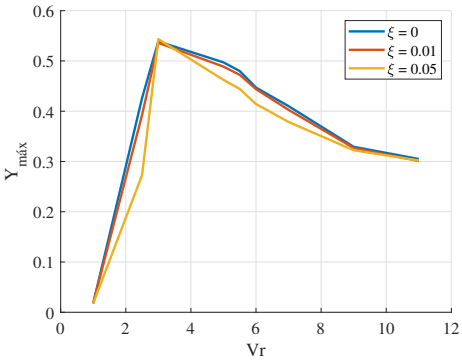

Figure 3. Maximum dimensionless amplitude as a function of the reduced velocity

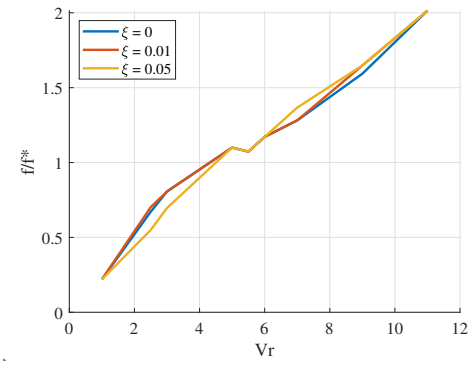

Figure 4. Frequency ratio as a function of the reduced velocity of the spring-mass-damper system

In Figure 3, where the dimensionless amplitude of the cylinder oscillation as a function of the reduced velocity is represented, it is possible to identify that the amplitude of the cylinder, when $1 < V_r < 2.5$, increases considerably. According to Williamson and Roshko (1988) [13], this response is identified as simple vortices (S), that is, for each period of oscillation of the cylinder, two vortices are released. Brika and Laneville (1993) [6] defined the 2S model as the upper branch, that is, for each period of cylinder oscillation, two singular vortices are released.From the reduced velocity $3.5 < V_r < 8.5$, it is observed that after reaching the maximum amplitude this value gradually decreases. All of this is due to the system's synchronization and, according to Williamson and Roshko (1988) [13], the vortices on the mat are also released according to the 2S pattern, but unlike the vortices released in the previous one. After the reduced velocity $V_r = 8$, the oscillation amplitude of the system abruptly changes to the lowest value.

Figure 4 illustrates the relationship between frequencies as a function of reduced velocity. It is verified that for reduced velocity $4.5 < V_r < 6$ and $V_r > 9$, the frequency is coincident, and it is possible to observe the overlap between the different damping rates.

It is possible to observe in Figures 3 and 4, that for the reduced velocity, it is verified that the response of the system with damping of $\xi = 0.01$ and $\xi = 0.05$ and the spring-mass system are very similar. This can be explained by the reason of the high values of spring stiffness and the damping constant of the systems, thus there is no significant difference in the system with or without damper.

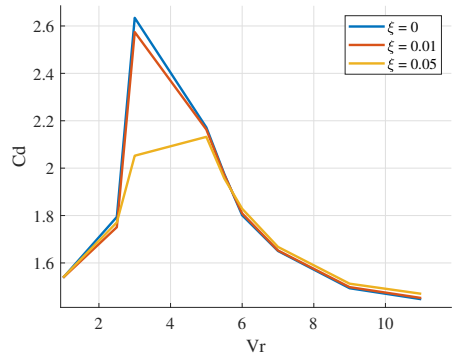

Figure 5. Mean of the drag coefficient as a function of the reduced velocity of the mass-spring-damper system

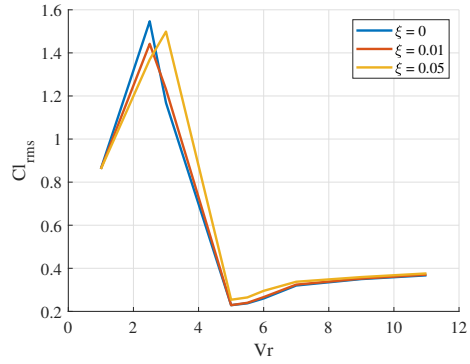

Figure 6. Standard deviation of the lift coefficient as a function of the reduced velocity of the mass-spring-damper system

In Figure 5, where the average drag coefficient for the mass-spring-damper system is represented, ensure that for the reduced velocity $V_r < 2.5$ the average drag coefficient is very similar in the three studied damping rates, being almost coincident. As mentioned earlier, the spring stiffness constant is too high, making the system very rigid and resulting in lower oscillation amplitude. From the reduced velocity, $V_r = 2.5$, it can be verified that the average drag coefficient of the two systems increased considerably. When the mass-spring-damping system with

damping rate, $\xi = 0.05$, approaches the reduced velocity, $V_r = 3.5$, there is a considerable decrease in the drag coefficient compared to the system with damping rate, $\xi = 0$ and $\xi = 0.01$.

The lift coefficient fluctuation by the reduced velocity is represented in Figure 6 where there is a small difference for reduced velocity, $2.5 > V_r > 4.5$, at the other reduced velocity. Despite the damping rate, the amplitude of the lift coefficient of the mass-spring and mass-spring-damper system has the same amplitudes.

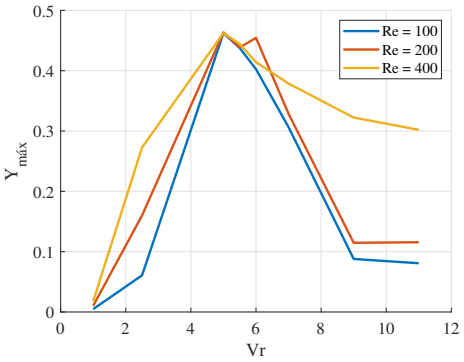

Figure 7. Maximum dimensionless amplitude as a function of the reduced velocity

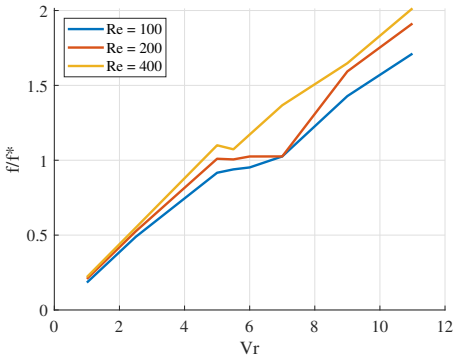

Figure 8. Frequency ratio as a function of the reduced velocity of the spring-mass-damper system

Figure 7 shows a comparison of the dimensionless amplitude of cylinder oscillation as a function of the reduced velocity for Reynolds of 100, 200 and 400, for a damping rate of $\xi = 0.05$. In this comparison, it is observed that there were points of intersection between $5 > V_r > 5.5$ for all Reynolds numbers, and a greater distance from the Reynolds 400 from the reduced speed of 6.5.

Figure 8 shows the comparison between the frequency ratios as a function of the reduced velocity of the mass-spring-damper system with different Reynolds numbers. It is possible to identify that there is a $f/f^* = 1$ plateau in the Reynolds 100 and 200 responses; however, there is a discrepancy between the Reynolds 400 in relation to the others. Still in this analysis, it appears that this divergence between the Reynolds numbers is directly influenced by the reduced velocities in the interval $5.5 > V_r > 5.8$, for Reynolds 400, and $5.5 > V_r > 6.5$, for Reynolds 100 and 200.

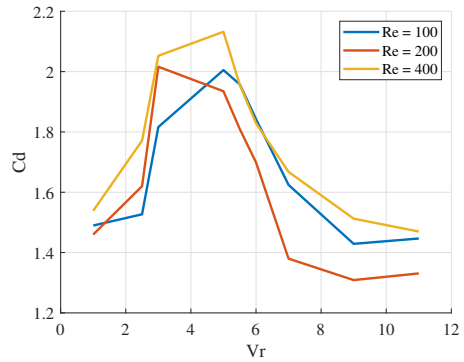

Figure 9. Mean of the drag coefficient as a function of the reduced velocity of the mass-spring-damper system

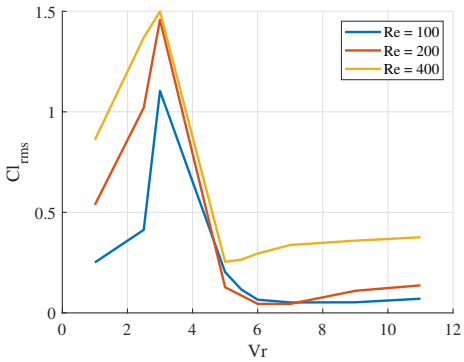

Figure 10. Standard deviation of the lift coefficient as a function of the reduced velocity of the mass-spring-damper system

Still, in the analysis of the damping rate $\xi = 0.05$, Figure 9, the graph shows the results of the drag coefficient C_d for Reynolds 100, 200 and 400. Note that the coefficients for different reduced speeds did not show uniformity between the C_d values. It is noteworthy that the reduced speeds directly impacted the results, leading to the oscillation seen in the graph.

Analyzing Figure 10, the results of the lift coefficient as a function of the reduced velocity in the Reynolds 100, 200 and 400, registered a slight approximation in the Reynolds 200 and 400 for the interval of $2.5 > V_r > 4.5$. Regarding the Reynolds 100 result, the behavior of the graph was very similar, but with lower values. This peak in system response corresponds to the phase angle change, which affects the vortex pattern released in the wake. An important observation is the direct influence of the Reynolds number in this analysis. It is observed that as the Reynolds increases there is a significant variation in the results, therefore, an increasing variation in the results.

5 Conclusions

The results obtained in the simulation of a flow around a fixed cylinder were the expected ones, however, in comparison with the literature, the importance of the dimensions of the computational domain is highlighted. The domain of the meshes used in this study is smaller than those used by other authors, therefore, there is a slight difference in the results of C_d, Cl_{rms} and St.

The results of the flow simulation around an oscillating cylinder were also satisfactory. Through the results obtained by the mass-spring systems and mass-spring-damper, it is concluded that, for low reduced speeds, the response of the system is very identical to the response of the fixed cylinder, this in relation to the C_d and Cl_{rms}. This is due to the high value of spring stiffness which makes the system very rigid, which makes the cylinder's oscillation amplitude low. Increasing the reduced speed, it is observed that the amplitude of cylinder oscillation takes on higher values, this response being different from the previous one. This jump in amplitude is due to the fact that the phase angle changes, causing the vortices released in the wake to be formed and released in a different way than for lower reduced velocities.

References

[1] R. M. Stringer, J. Zang, and A. J. Hillis. Unsteady RANS computations of flow around a circular cylinder for a wide range of Reynolds numbers. *Ocean Engineering*, vol. 87, pp. 1–9, 2014.
[2] D. Cóstola and M. P. Alucci. Application of CFD simulations for the calculation of external wind pressure coefficients on openings of a building. *Ambiente Construído*, vol. 11, n. 1, pp. 145–158, 2011.
[3] G. Palau-Salvador, T. Stoesser, J. Fröhlich, M. Kappler, and W. Rodi. Large eddy simulations and experiments of flow around finite-height cylinders. *Flow, Turbulence and Combustion*, vol. 84, n. 2, pp. 239–275, 2010.
[4] T. Sarpkaya. Vortex-induced oscillations - a selective review. *ASME, Transactions, Journal of Applied Mechanics*, vol. 46, pp. 241–258, 1979.
[5] P. W. Bearman. Vortex shedding from oscillating bluff bodies. *Annual Review of Fluid Mechanics*, vol. 16, n. 1, pp. 195–222, 1984.
[6] D. Brika and A. Laneville. Vortex-induced vibrations of a long flexible circular cylinder. *Journal of Fluid Mechanics*, vol. 250, n. EM5, pp. 481–508, 1993.
[7] T. Sarpkaya. A critical review of the intrinsic nature of vortex-induced vibrations. *Journal of fluids and structures*, vol. 19, n. 4, pp. 389–447, 2004.
[8] M. Belloli, S. Giappino, S. Morganti, S. Muggiasca, and A. Zasso. Vortex induced vibrations at high reynolds numbers on circular cylinders. *Ocean engineering*, vol. 94, pp. 140–154, 2015.
[9] R. D. Blevins. *Flow-Induced Vibration*, 2001.
[10] C. K. Vikram. Analysis by CFD for flow past circular and square cylinder. *International Journal of Innovations in Engineering and Technology*, vol. 4, n. 3, pp. 72–76, 2014.
[11] L. B. Junior. Estudo numérico do escoamento ao redor de um cilindro fixo. Master's thesis, Universidade de São Paulo, 2007.
[12] R. Franke, W. Rodi, and B. Schönung. Numerical calculation of laminar vortex-shedding flow past cylinders. *Journal of wind engineering and industrial aerodynamics*, vol. 35, n. C, pp. 237–257, 1990.
[13] C. Williamson and A. Roshko. Vortex formation in the wake of an oscillating cylinder. *Journal of fluids and structures*, vol. 2, n. 4, pp. 355–381, 1988.